A MUSCL–scheme on staggered grids with kinetic–like fluxes for the barotropic Euler system

Thierry Goudon*[1], Julie Llobell†[1], and Sebastian Minjeaud‡[1]

[1]Université Côte d'Azur, Inria, CNRS, LJAD,
Parc Valrose, F-06108 Nice, France

Abstract

We set up a MUSCL version of the scheme introduced in [F. Berthelin, T. Goudon, S. Minjeaud, Math. Comput. (84)2015, pp. 2221–2262] for solving the barotropic Euler equations. The scheme works on staggered grids, with numerical densities and velocities stored at dual locations, while the numerical fluxes are derived in the spirit of kinetic schemes. We identify stability conditions for the second order method. We illustrate the ability of the scheme to capture the structure of complex flows with 2D simulations on MAC grids.

Keywords: Finite Volume schemes MUSCL methods Staggered grids Kinetic schemes Euler equations

MSC Class.: 65M08 35L65 35Q31 76M12

1 Introduction

This work is concerned with the numerical solution of the barotropic Euler system

$$\begin{cases} \partial_t \rho + \operatorname{div}\big(\rho \mathbf{u}\big) = 0, \\ \partial_t \big(\rho \mathbf{u}\big) + \operatorname{div}\big(\rho \mathbf{u} \otimes \mathbf{u}\big) + \nabla\big(p(\rho)\big) = 0. \end{cases} \tag{1}$$ euler

This model describes the evolution of a compressible fluid (in the absence of external forces). The unknowns ρ and $\mathbf{u}$ stand respectively for the local density and velocity field of the fluid. They depend on the time and space variables, $t \geqslant 0$ and $x \in \mathbb{R}^N$. The

*thierry.goudon@inria.fr
†julie.llobell@unice.fr
‡minjeaud@unice.fr

model assumes that the pressure p depends on the density ρ only. Here and below, we suppose that the pressure law $\rho \mapsto p(\rho)$ belongs to $\mathcal{C}^2([0,\infty))$ and satisfies

$$p(\rho) > 0, \quad p'(\rho) > 0, \quad p''(\rho) > 0, \qquad \forall \rho > 0. \tag{2}$$ pressure

For instance, these properties hold for the classical power–law $p(\rho) = a\rho^\gamma$ with $a > 0$ and $\gamma > 1$. We refer the reader to the classical treatises [8, 17, 21, 28, 36] for a thorough introduction to these equations and for a description of the numerical issues. Bouc,Daf, GodR, Leveq, tor-09-rie

We are interested in numerical schemes for (1) defined on staggered grids. To be more specific, let us focus on the one-dimensional case where x lies in the slab $[0, L] \subset \mathbb{R}$. To define the discrete unknowns, we proceed as follows, see Fig. 1: euler FigMesh

- we introduce a set of $J+1$ points $x_1 = 0 < x_2 < ... < x_J < x_{J+1} = L$ in the computational domain; we denote by $\mathcal{C}_{j+\frac{1}{2}} = [x_j, x_{j+1}]$, $j \in [\![1, J]\!]$, the cells defined by these points;
- we denote by $x_{j+\frac{1}{2}} = (x_j + x_{j+1})/2$, $j \in [\![1, J]\!]$, the centers of the cells; these points define the dual cells $\mathcal{C}_j = [x_{j-\frac{1}{2}}, x_{j+\frac{1}{2}}]$, $j \in [\![2, J]\!]$;
- we set the following notation for the mesh-sizes

$$\delta x_{j+\frac{1}{2}} = x_{j+1} - x_j, \ j \in [\![1, J]\!], \quad \text{and} \quad \delta x_j = \frac{\delta x_{j-\frac{1}{2}} + \delta x_{j+\frac{1}{2}}}{2}, \ j \in [\![2, J]\!],$$

  (with the specific definition for the end–cells: $\delta x_1 = \frac{1}{2}\delta x_{\frac{3}{2}}$ and $\delta x_{J+1} = \frac{1}{2}\delta x_{J+\frac{1}{2}}$).

We have in mind the derivation of Finite Volume schemes where the discrete densities are thought of as approximation of the density ρ on the cells $\mathcal{C}_{j+\frac{1}{2}}$ and the discrete velocities u_j are thought of as approximation of the velocity u on the cells $\mathcal{C}_j$. Therefore the scheme has the general form

- for the mass equation

$$\frac{\delta x_{j+\frac{1}{2}}}{\delta t}(\rho^{k+1}_{j+\frac{1}{2}} - \rho^k_{j+\frac{1}{2}}) + \mathcal{F}^k_{j+1} - \mathcal{F}^k_j = 0, \qquad \forall j \in [\![1, J]\!],$$

- for the momentum equation :

$$\frac{\delta x_j}{\delta t}(\rho^{k+1}_j u^{k+1}_j - \overline{\rho}^k_j u^k_j) + \tilde{\mathcal{F}}^k_{j+\frac{1}{2}} - \tilde{\mathcal{F}}^k_{j-\frac{1}{2}} = 0, \qquad \forall j \in [\![2, J]\!]$$

  where ρ_j, $j \in [\![2, J]\!]$ are approximations of ρ at the internal edges of the primal mesh:

$$\rho_j = \frac{\delta x_{j+\frac{1}{2}}\rho_{j+\frac{1}{2}} + \delta x_{j-\frac{1}{2}}\rho_{j-\frac{1}{2}}}{2\delta x_j}.$$

Of course, the scheme has to be completed by initial and boundary conditions.

Usually, the system (1) is treated using a vector–valued unknown $U = (\rho, u)$ stored on a colocalized grid. The use of staggered grids is less standard, with the motivation of having a unified approach with an incompressible code, see e.g. [37, 39, 40, 41]. In particular, colocalized approaches may lead to instabilities in Low–Mach regimes, with euler Wes3, Hof, Wes1,Wes2

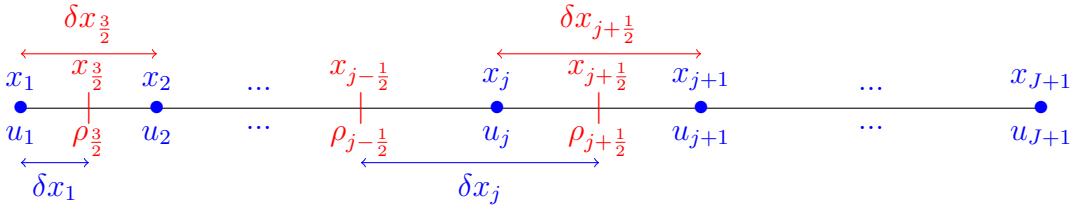

FigMesh

Figure 1: Staggered grid in dimension one.

spurious oscillations of the pressure due to an "odd–even decoupling", see [GHK, HKL, HLN, HLN2, Zaz] [20, 24, 25, 26, 42]. For the same reasons, the choice of a staggered discretization is motivated in [BGM,BGM2] [4, 5] by further applications to the simulations of mixture flows where the models also involve a solenoidal constraint, see also [CDNR, CDNR2, Polizzi] [13, 14, 33] and the references therein. Coupled with a projection approach, the staggered method makes the discretization of the mass conservation equations for all the species interacting in the mixture and the definition of the pressure field compatible.

In contrast to the colocalized approach (with the noticeable exception of AUSM schemes [AUSM, AUSM2] [30, 29]), a discretization of each physical variables, ρ and $\mathbf{u}$ separately, is natural on a staggered grid. In particular, the mass flux $\mathcal{F}_j$ at the interface x_j can use directly the material velocity u_j. For instance, it looks tempting to define the flux $\mathcal{F}_j$ based on the UpWinding principles according to the sign of u_j, see [HLN,HLN2] [25, 26] but this approach does not use the hyperbolic properties of the system ([euler] 1) and it might lead to spurious oscillations, see [BGM] [4, Appendix B]. Instead, the flux designed in [BGM, BGM2] [4, 5] makes full use of the characteristic speeds of the system ([euler] 1), namely

$$u \pm c(\rho), \qquad \text{with } c(\rho) = \sqrt{p'(\rho)}, \text{ the sound speed.}$$

The formula for the numerical flux in [BGM, BGM2] [4, 5] comes from the integration of a certain equilibrium function over a "ghost" velocity variable, in the spririt of the kinetic schemes, see [CoPe, Desh, Desh2, Kan, PerBS, Pulin] [16, 18, 19, 27, 32, 34]. The integration domain is delimited by the characteristic speeds in order to enforce the stability of the scheme, according to an idea that dates back to [Kan] [27]. Finally, the numerical mass flux in [BGM, BGM2] [4, 5] is defined by the following formula

$$\mathcal{F}_j = \mathcal{F}^+(\rho_{j-\frac{1}{2}}, u_j) + \mathcal{F}^-(\rho_{j+\frac{1}{2}}, u_j), \qquad j \in [\![2, J]\!],$$

(and $\mathcal{F}_1 = 0 = \mathcal{F}_{J+1}$ if the zero flux boundary condition is prescribed) with

$$\mathcal{F}^+(\rho, u) = \begin{cases} 0 & \text{if } u \leqslant -c(\rho), \\ \dfrac{\rho}{4c(\rho)}(u + c(\rho))^2 & \text{if } |u| < c(\rho), \\ \rho u & \text{if } u > c(\rho), \end{cases} \tag{3}$$

fluxp

and

$$\mathcal{F}^-(\rho, u) = \begin{cases} \rho u & \text{if } u \leqslant -c(\rho), \\ -\dfrac{\rho}{4c(\rho)}(u - c(\rho))^2 & \text{if } |u| < c(\rho), \\ 0 & \text{if } u > c(\rho). \end{cases} \tag{4}$$

fluxm

We note that a symmetry property holds

$$\mathcal{F}^-(\rho,u) = -\mathcal{F}^+(\rho,-u),$$

and it is clear that the flux–consistency condition is fulfilled

$$\mathcal{F}^+(\rho,u) + \mathcal{F}^-(\rho,u) = \rho u. \tag{5}$$

eq:mass_consit

It is worth having in mind Fig. 2, which clarifies the correction with respect to the mere UpWind flux based on the sign of the material velocity. As explained in [4], it induces some numerical diffusion which prevents the formation of oscillations in the vicinity of small material velocities.

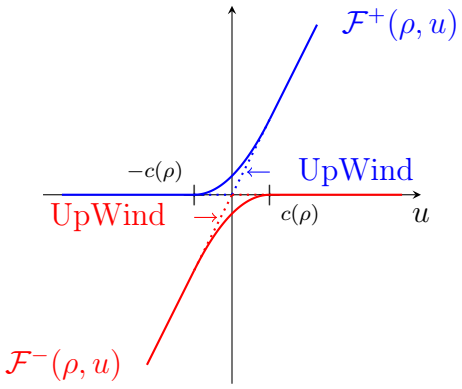

Figure 2: Comparison of the flux (3)–(4) and the UpWind flux for a fixed ρ.

FigFlux

For the momentum flux, the pressure gradient at $x_{j+\frac{1}{2}}$ is naturally centered by using the densities in the neighboring cells, while the convection flux is written by applying the upwinding principle, based on the "sign" of the mass fluxes $\mathcal{F}_j$ and $\mathcal{F}_{j+1}$, to the velocity field. We arrive at the following definition

$$\tilde{\mathcal{F}}_{j+\frac{1}{2}} = \mathcal{G}_{j+\frac{1}{2}} + p(\rho_{j+\frac{1}{2}}),$$

with

$$\mathcal{G}_{j+\frac{1}{2}} = \frac{u_j}{2}\left(\mathcal{F}^+(\rho_{j-\frac{1}{2}},u_j) + \mathcal{F}^+(\rho_{j+\frac{1}{2}},u_{j+1})\right) + \frac{u_{j+1}}{2}\left(\mathcal{F}^-(\rho_{j+\frac{1}{2}},u_j) + \mathcal{F}^-(\rho_{j+\frac{3}{2}},u_{j+1})\right),$$

(and a convenient definition of the boundary terms). It is clear that, due to (5), the momentum flux is also consistent.

eq:mass_consit

The scheme has the following properties and abilities, at least in this simple 1D framework:

- stability analysis [4]: up to a (quite standard) stability condition on the numerical parameters, the scheme preserves the positivity of the density, and it makes the total energy of the system decay,

- consistency analysis [BGM3]: the scheme satisfies a Lax–Wendroff type theorem,
- simulations: the scheme has the advantage of algorithmic simplicity (it does not require to solve Riemann problems and the definition of the flux (3)–(4) is fully explicit; despite its "kinetic" flavor, it does not require an additional integration procedure...), it performs well on the standard test cases of Riemann problems and it works for very general pressure laws, like with close–packing pressures, see [BGM, BGM2] [4, 5].

We wish to propose a second order extension of this scheme, by adapting the MUSCL principles [BVL] [38] to the staggered framework.

This work is organized as follows. We start by explaining in Section 2 [DefSch] the adaptation of the MUSCL procedure to the staggered scheme. As explained above, for the mass flux the velocity is already stored at the interface and we only need to reconstruct a suitable interface density. We combine the modified mass flux and a reconstruction of the velocity to define the momentum fluxes. We are able to identify the stability condition which ensures the preservation of the positivity of the density by the MUSCL scheme, and we justify that the construction reaches formally the second order accuracy. In Section 3, [Sec2d] we briefly explain how to extend the 1D scheme to higher dimensions, when working with Cartesian grids. The staggered framework then naturally leads to a MAC–like discretization, in the spirit of the pioneering work [HW] [23] for incompressible flows. Section 4 [Simul] is devoted to numerical validations. We check numerically the gain of accuracy on explicit solutions and on 1D Riemann problems. Then we address 2D cases, like the simulation of falling columns by the Shallow Water system, as proposed in [Agu] [1], and the forward facing step inspired from [CW] [15].

2 A MUSCL scheme on staggered grids

DefSch

In this section we discuss how we adapt the MUSCL procedure to the staggered grids. Concerning the discretization of the mass flux, we keep unchanged the velocity defined at the interface x_j and we shall replace the UpWind value $\rho_{j\pm\frac{1}{2}}$ by a MUSCL reconstruction $\rho_j^{\pm}$ of the density: it defines the upgraded mass flux $\mathcal{F}_j^{ML}$. For the momentum flux, since the discretization of the pressure is centered, we only need to define the convection flux $\mathcal{G}_{j+\frac{1}{2}}^{ML}$: we shall combine the obtained mass fluxes $\mathcal{F}_j^{ML}$ and $\mathcal{F}_{j+1}^{ML}$ with a MUSCL reconstructed velocity $V_{j+\frac{1}{2}}^{\pm}$ at the interfaces $x_{j+\frac{1}{2}}$.

2.1 Definition of the scheme

We introduce a piecewise linear reconstruction of the density which is defined, on each cell $\mathcal{C}_{j+\frac{1}{2}}$, $j \in [\![1, J]\!]$, by

$$\hat{\rho}_{j+\frac{1}{2}}(x) = \rho_{j+\frac{1}{2}} + s_{j+\frac{1}{2}}(x - x_{j+\frac{1}{2}}), \qquad \forall x \in \mathcal{C}_{j+\frac{1}{2}}.$$

The slope $s_{j+\frac{1}{2}} \in \mathbb{R}$ should be defined as an approximation of the density gradient in the cell $\mathcal{C}_{j+\frac{1}{2}}$. It is thus set as a symmetric function of the two discrete derivatives

computed using the values of the density on the neighboring cells,

$$s_{j+\frac{1}{2}} = \widehat{\Phi}\Big(\frac{\rho_{j+\frac{1}{2}} - \rho_{j-\frac{1}{2}}}{\delta x_j},\ \frac{\rho_{j+\frac{3}{2}} - \rho_{j+\frac{1}{2}}}{\delta x_{j+1}}\Big), \qquad \forall j \in [\![2, J-1]\!].$$

For $j = 1$ and $j = J$, the above formula should be modified according to the boundary conditions. Here, we simply take $s_{\frac{3}{2}} = 0$ and $s_{J+\frac{1}{2}} = 0$ (which makes the scheme degenerate to first order next to the boundaries).

For stability reasons, in order to prevent the formation of over- and undershoots, the value of the reconstructed densities at an edge should not exceed the values of the density in the two neighboring cells and the slope $s_{j+\frac{1}{2}}$ should vanish at extrema. These properties are classically ensured by the definition of the function $\widehat{\Phi}$, the so-called limiter function. It is seen here as a function of two variables (a, b) but it is also customary to use instead a function Φ of the single variable a/b with the following equalities

$$\widehat{\Phi}(a, b) = b\ \Phi\Big(\frac{a}{b}\Big) = a\ \Phi\Big(\frac{b}{a}\Big) = \widehat{\Phi}(b, a),$$

where it is understood that the function Φ satisfies the symmetry property

$$\frac{\Phi(r)}{r} = \Phi\Big(\frac{1}{r}\Big),\ \forall r \neq 0. \tag{6}$$ eq:sym_limiteur

On uniform grids, the geometric properties stated above are ensured when the limiter function lies in the well–known Sweby TVD region, see [38, 35], which is characterized by the three conditions BVL,Swe

$$\underbrace{\Phi(r) = 0}_{(a)},\ \forall r \leqslant 0, \qquad \underbrace{0 \leqslant}_{(b)} \Big(\Phi(r), \frac{\Phi(r)}{r}\Big) \underbrace{\leqslant 2}_{(c)},\ \forall r \geqslant 0.$$

On non-uniform grids, the situation is more intricate as explained in [2]: in condition BAM (c) the upper bound 2 should be replaced by a quantity that depends on the mesh regularity. More precisely the limiter Φ must satify

$$\Phi(r) = 0,\ \forall r \leqslant 0, \qquad 0 \leqslant \Big(\Phi(r), \frac{\Phi(r)}{r}\Big) \leqslant \tau,\ \forall r \geqslant 0, \tag{7}$$ eq:tvd_limiteur

where $1 < \tau \leqslant 2$ is the mesh dependent number defined by

$$\tau = \min_{j \in [\![2, J-1]\!]} \Big(\frac{2\delta x_j}{\delta x_{j+\frac{1}{2}}}; \frac{2\delta x_{j+1}}{\delta x_{j+\frac{1}{2}}}\Big).$$

Furthermore, in order to ensure that the scheme is second order in space (see Section 2.2 below), the limiter function $r \mapsto \Phi(r)$ should be a smooth function — with at least left and right derivatives at the point $r = 1$ — and satisfy sec:analysis

$$\Phi(1) = 1. \tag{8}$$ eq:snd_limiteur

As discussed in Lemma 2.5 (in Section 2.2 below), if $x \mapsto \rho(x)$ is a smooth function, the derivatives of which are bounded and remain bounded, denoting $\rho_{j+\frac{1}{2}} = \rho(x_{j+\frac{1}{2}})$, then we get

$$s_{j+\frac{1}{2}} = \rho'(x_{j+\frac{1}{2}}) + \mathcal{O}(\delta x).$$

From classical limiters defined for uniform meshes, we can define τ-limiters that satisfy properties (6), (7) and (8), see [12].

exe

Example 2.1. Examples of flux limiters and their associated τ-limiters:

- The MinMod limiter : $\Phi_{mm}(r) = \max[0, \min[1, r]]$, which is actually upper–bounded by 1,
- and the τ-MinMod limiter : $\Phi_{\tau-mm}(r) = \max[0, \min[\tau, r]]$,
- The SuperBee limiter : $\Phi_{sb}(r) = \max[0, \min(2r, 1), \min(r, 2)]$,
- and the τ-Bee limiter : $\Phi_{\tau-sb}(r) = \max[0, \min(\tau r, 1), \min(r, \tau)]$.

A similar reconstruction is used for the velocity on the dual mesh. We set

$$\widehat{V}_j(x) = V_j + w_j(x - x_j), \quad \forall x \in \mathcal{C}_j, \quad \forall j \in [\![1, J+1]\!].$$

The slopes $w_j \in \mathbb{R}$ are now defined by

$$w_j = \widehat{\Phi}\left(\frac{V_j - V_{j-1}}{\delta x_{j-\frac{1}{2}}}, \frac{V_{j+1} - V_j}{\delta x_{j+\frac{1}{2}}}\right), \quad \forall j \in [\![2, J]\!], \qquad \text{and} \qquad w_1 = 0 = w_{J+1}.$$

The affine reconstruction $\hat{\rho}$ of the density allows us to define the two values $\rho_j^- = \hat{\rho}_{j-\frac{1}{2}}(x_j)$ and $\rho_j^+ = \hat{\rho}_{j+\frac{1}{2}}(x_j)$ at the interface x_j,

$$\rho_j^- = \rho_{j-\frac{1}{2}} + \frac{\delta x_{j-\frac{1}{2}}}{2}\, s_{j-\frac{1}{2}}, \quad \forall j \in [\![2, J+1]\!],$$
$$\rho_j^+ = \rho_{j+\frac{1}{2}} - \frac{\delta x_{j+\frac{1}{2}}}{2}\, s_{j+\frac{1}{2}}, \quad \forall j \in [\![1, J]\!].$$

In the same way, the affine reconstruction of the velocity $\widehat{V}$ allows us to define $V_{j+\frac{1}{2}}^- = \widehat{V}_j(x_{j+\frac{1}{2}})$ and $V_{j+\frac{1}{2}}^+ = \widehat{V}_{j+1}(x_{j+\frac{1}{2}})$ at the interfaces $x_{j+\frac{1}{2}}$,

$$V_{j+\frac{1}{2}}^- = V_j + \frac{\delta x_{j+\frac{1}{2}}}{2}\, w_j, \qquad \forall j \in [\![2, J]\!],$$
$$V_{j+\frac{1}{2}}^+ = V_{j+1} - \frac{\delta x_{j+\frac{1}{2}}}{2}\, w_{j+1}, \qquad \forall j \in [\![1, J-1]\!].$$

Here, we bear in mind that x_j and x_{j+1} are not necessarily the mid–points of $\mathcal{C}_j$ and $\mathcal{C}_{j+1}$ respectively; this is the reason why the formula is not expressed by means of $\delta x_{j+1}/2$ and $\delta x_j/2$.

Finally, we can now define the modified fluxes. We update the density by replacing the mass flux $\mathcal{F}_j$ by the MUSCL–flux $\mathcal{F}_j^{ML}$ defined by

$$\mathcal{F}_j^{ML} = \mathcal{F}^+(\rho_j^-, V_j) + \mathcal{F}^-(\rho_j^+, V_j), \qquad \forall j \in [\![2, J]\!],$$

(and $\mathcal{F}_1^{ML} = 0 = \mathcal{F}_{J+1}^{ML}$ if the zero-flux condition is imposed). We naturally set

$$\mathcal{F}_j^{ML,+} = \mathcal{F}^+(\rho_j^-, V_j) \text{ and } \mathcal{F}_j^{ML,-} = \mathcal{F}^-(\rho_j^+, V_j).$$

The convection part of the momentum flux is given by

$$\mathcal{G}_{j+\frac{1}{2}}^{ML} = V_{j+\frac{1}{2}}^- \frac{\mathcal{F}_j^{ML,+} + \mathcal{F}_{j+1}^{ML,+}}{2} + V_{j+\frac{1}{2}}^+ \frac{\mathcal{F}_j^{ML,-} + \mathcal{F}_{j+1}^{ML,-}}{2}, \qquad \forall j \in [\![2, J-1]\!]. \tag{9}$$

eq:fluxQDM

We set $\mathcal{G}_{\frac{3}{2}}^{ML} = \dfrac{V_{\frac{3}{2}}^+}{2} \mathcal{F}_2^{ML,-}$ and $\mathcal{G}_{J+\frac{1}{2}}^{ML} = \dfrac{V_{J+\frac{1}{2}}^-}{2} \mathcal{F}_J^{ML,+}$ for the boundary values.

Remark 2.2. It is worth mentioning here the recent work [6, 7] by C. Berthon, Y. Coudière and V. Desveaux who develop a high order scheme for the Euler system by doubling the set of numerical unknowns: the conserved quantities $U = (\rho, \rho\mathbf{u})$ are stored on both the primal and the dual cells. This approach is very appealing in the multi–dimensional case since it provides naturally a way to define full gradients on the interface of the control volumes of an unstructured mesh. This idea might be equally relevant for dealing with the full Euler system where the total energy mixes the kinetic energy and the internal energy, see [22]. Note also that the definition of limiters on general unstructured meshes gives rise to challenging issues, see [12, 9, 10] and the references therein. Here we are only concerned with the simpler situation of Cartesian grids and the scheme does not need to double all variables. Note also that in the present framework it is more adapted to work with the physical quantities ρ and $\mathbf{u}$.

2.2 Stability and consistency analysis

sec:analysis

Firstly, we exhibit a CFL-condition which ensures that the numerical density remains non–negative and, secondly, we investigate the consistency of the scheme, showing it can reach the second order accuracy for smooth solutions.

Rho-pos

Proposition 2.3 (Maximum principle for the density)**.** *Suppose that the limiter function Φ satisfy (7) and that the initial data satisfies $\rho_{j+\frac{1}{2}}^0 \geqslant 0$ for all $j \in [\![1, J]\!]$. We assume the CFL-like condition*

$$\frac{\delta t}{\delta x_{j+\frac{1}{2}}} \left(\left[\lambda_-(\rho_j^{k,+}, V_j^k) \right]^- + \left[\lambda_+(\rho_{j+1}^{k,-}, V_{j+1}^k) \right]^+ \right) \leqslant \frac{1}{2}, \quad \forall j \in [\![1, J]\!], \tag{10}$$

eq:cfl

at every time step. Then the scheme preserves the non–negativity of the density:

$$\rho_{j+\frac{1}{2}}^{k+1} \geqslant 0 \text{ for all } j \in [\![1, J]\!] \text{ and } k \in \mathbb{N}.$$

Proof. We assume that $\rho^k_{j+\frac{1}{2}} \geqslant 0$ holds for all $j \in [\![1, J]\!]$. Let us introduce the following quantities

$$\alpha^k_j = \frac{\delta x_{j+\frac{1}{2}}}{2\delta x_j}\ \Phi\left(\frac{\rho^k_{j+\frac{3}{2}} - \rho^k_{j+\frac{1}{2}}}{\delta x_{j+1}} \frac{\delta x_j}{\rho^k_{j+\frac{1}{2}} - \rho^k_{j-\frac{1}{2}}}\right),$$

and

$$\beta^k_j = \frac{\delta x_{j+\frac{1}{2}}}{2\delta x_{j+1}}\ \Phi\left(\frac{\rho^k_{j+\frac{1}{2}} - \rho^k_{j-\frac{1}{2}}}{\delta x_j} \frac{\delta x_{j+1}}{\rho^k_{j+\frac{3}{2}} - \rho^k_{j+\frac{1}{2}}}\right).$$

Owing to property (7), we readily check that $0 \leqslant \alpha^k_j \leqslant 1$ and $0 \leqslant \beta^k_j \leqslant 1$. Furthermore, the reconstructed densities can be equivalently recast as

$$\rho^{k,+}_j = (1-\alpha^k_j)\rho^k_{j+\frac{1}{2}} + \alpha^k_j \rho^k_{j-\frac{1}{2}} \quad \text{and} \quad \rho^{k,-}_{j+1} = (1+\alpha^k_j)\rho^k_{j+\frac{1}{2}} - \alpha^k_j \rho^k_{j-\frac{1}{2}}, \tag{11}$$

or

$$\rho^{k,+}_j = (1+\beta^k_j)\rho^k_{j+\frac{1}{2}} - \beta^k_j \rho^k_{j+\frac{3}{2}} \quad \text{and} \quad \rho^{k,-}_{j+1} = (1-\beta^k_j)\rho^k_{j+\frac{1}{2}} + \beta^k_j \rho^k_{j+\frac{3}{2}}. \tag{12}$$

In particular, equalities (11) show that

$$\rho^{k,+}_j \geqslant \min\left(\rho^k_{j-\frac{1}{2}}, \rho^k_{j+\frac{1}{2}}\right) \geqslant 0, \quad \text{and} \quad \rho^{k,-}_{j+1} \leqslant 2\rho^k_{j+\frac{1}{2}},$$

and equalities (12) show that

$$\rho^{k,+}_j \leqslant 2\rho^k_{j+\frac{1}{2}}, \quad \text{and} \quad \rho^{k,-}_{j+1} \geqslant \min\left(\rho^k_{j-\frac{1}{2}}, \rho^k_{j+\frac{1}{2}}\right) \geqslant 0.$$

Reasoning now as in [4, Lemma 3.7], using the sign property of the flux functions $\pm\mathcal{F}^{\pm} \geqslant 0$, we are led to the following estimate

$$\rho^{k+1}_{j+\frac{1}{2}} \geqslant \rho^k_{j+\frac{1}{2}} + \frac{\delta t}{\delta x_{j+\frac{1}{2}}}\left(\mathcal{F}^-(\rho^{k,+}_j, V^k_j) - \mathcal{F}^+(\rho^{k,-}_{j+1}, V^k_{j+1})\right).$$

Owing to [4, Lemma 3.3] and since $\rho^+_j \geqslant 0$ and $\rho^-_{j+1} \geqslant 0$, we obtain

$$\rho^{k+1}_{j+\frac{1}{2}} \geqslant \rho^k_{j+\frac{1}{2}} - \frac{\delta t}{\delta x_{j+\frac{1}{2}}}\left(\rho^{k,+}_j \left[\lambda_-(\rho^{k,+}_j, V^k_j)\right]^- + \rho^{k,-}_{j+1}\left[\lambda_+(\rho^{k,-}_{j+1}, V^k_{j+1})\right]^+\right).$$

Next, bearing in mind that $\rho^+_j \leqslant 2\rho^k_{j+\frac{1}{2}}$ and $\rho^-_{j+1} \leqslant 2\rho^k_{j+\frac{1}{2}}$, we find

$$\rho^{k+1}_{j+\frac{1}{2}} \geqslant \rho^k_{j+\frac{1}{2}}\left(1 - \frac{2\delta t}{\delta x_{j+\frac{1}{2}}}\left(\left[\lambda_-(\rho^{k,+}_j, V^k_j)\right]^- + \left[\lambda_+(\rho^{k,-}_{j+1}, V^k_{j+1})\right]^+\right)\right).$$

Since it is assumed that $\rho^k_{j+\frac{1}{2}} \geqslant 0$, the conclusion $\rho^{k+1}_{j+\frac{1}{2}} \geqslant 0$ is obtained as a consequence of (10). □

Remark 2.4. It is worth pointing out that the CFL condition for the MUSCL scheme is twice more constrained than with the first order scheme in [4, Prop. 3.7]. This is due to the estimate $\rho^+_j \leqslant 2\rho_{j+\frac{1}{2}}$ and $\rho^-_{j+1} \leqslant 2\rho_{j+\frac{1}{2}}$.

Next, we wish to investigate the consistency of the scheme, showing it can reach the second order accuracy for smooth solutions, and far away from extrema. To this end, we study (at a fixed time) the consistency of the mass and momentum fluxes. The time being fixed, we consider smooth functions $\bar\rho$ and $\bar V$ of the space variable x only (say of class C^1 with bounded and not vanishing derivatives). We set $\bar\rho_{j+\frac12} = \bar\rho(x_{j+\frac12})$ and $\bar V_j = \bar V(x_j)$ and insert these quantities in the scheme instead of $\rho_{j+\frac12}$ and V_j. We denote with a bar all the quantities (slopes, reconstructed densities and velocities, fluxes...) defined in this way from $\bar\rho_{j+\frac12}$ and $\bar V_j$. The first observation, stated in Lemma 2.5, is that the reconstructed densities $\bar\rho_j^\pm$ and velocities $\bar V_{j+\frac12}^\pm$ are second order approximations of $\bar\rho(x_j)$ and $\bar V(x_{j+\frac12})$, respectively.

Lemma 2.5. *The following equalities hold:*

$$\bar\rho_j^+ = \bar\rho(x_j) + \mathcal{O}(\delta x^2),\ \forall j \in [\![1, J-1]\!], \qquad \bar\rho_j^- = \bar\rho(x_j) + \mathcal{O}(\delta x^2),\ \forall j \in [\![2, J]\!], \quad (13)$$

$$\bar V_{j+\frac12}^+ = \bar V(x_{j+\frac12}) + \mathcal{O}(\delta x^2),\ \forall j \in [\![1, J-1]\!],\ \bar V_{j+\frac12}^- = \bar V(x_{j+\frac12}) + \mathcal{O}(\delta x^2),\ \forall j \in [\![2, J]\!]. \quad (14)$$

Proof. We first prove that

$$\bar s_{j+\frac12} = \bar\rho'\big(x_{j+\frac12}\big) + \mathcal{O}\big(\delta x\big). \quad (15)$$

Indeed, we clearly have

$$\frac{\bar\rho_{j+\frac12} - \bar\rho_{j-\frac12}}{\delta x_j} = \bar\rho'\big(x_{j+\frac12}\big) + \mathcal{O}(\delta x), \quad \text{and} \quad \frac{\bar\rho_{j+\frac32} - \bar\rho_{j+\frac12}}{\delta x_{j+1}} = \bar\rho'\big(x_{j+\frac12}\big) + \mathcal{O}(\delta x),$$

so that

$$\frac{\bar\rho_{j+\frac32} - \bar\rho_{j+\frac12}}{\delta x_{j+1}} \frac{\delta x_j}{\bar\rho_{j+\frac12} - \bar\rho_{j-\frac12}} = 1 + \mathcal{O}\big(\delta x\big).$$

Since $\Phi(1) = 1$ and $r \mapsto \Phi(r)$ admits left and right derivatives at the point $r = 1$ (*cf.* assumption (8)), we get

$$\Phi\left(\frac{\bar\rho_{j+\frac32} - \bar\rho_{j+\frac12}}{\delta x_{j+1}} \frac{\delta x_j}{\bar\rho_{j+\frac12} - \bar\rho_{j-\frac12}}\right) = 1 + \mathcal{O}\big(\delta x\big).$$

This last equality together with the definition of $\bar s_{j+\frac12}$

$$\bar s_{j+\frac12} = \frac{\bar\rho_{j+\frac12} - \bar\rho_{j-\frac12}}{\delta x_j} \Phi\left(\frac{\bar\rho_{j+\frac32} - \bar\rho_{j+\frac12}}{\delta x_{j+1}} \frac{\delta x_j}{\bar\rho_{j+\frac12} - \bar\rho_{j-\frac12}}\right),$$

proves (15). Next, from (15) and the definition of $\bar\rho_j^\pm$ we readily find, for all $j \in [\![1, J]\!]$,

$$\bar\rho_{j+1}^- = \bar\rho_{j+\frac12} + \frac{\delta x_{j+\frac12}}{2}\ \bar\rho'\big(x_{j+\frac12}\big) + \mathcal{O}\big(\delta x^2\big),$$
$$\bar\rho_j^+ = \bar\rho_{j+\frac12} - \frac{\delta x_{j+\frac12}}{2}\ \bar\rho'\big(x_{j+\frac12}\big) + \mathcal{O}\big(\delta x^2\big).$$

The conclusion is then obtained using the following identities, direct consequences of the Taylor-Young expansion,

$$\bar{\rho}(x_{j+1}) = \bar{\rho}_{j+\frac{1}{2}} + \frac{\delta x_{j+\frac{1}{2}}}{2}\,\bar{\rho}'\big(x_{j+\frac{1}{2}}\big) + \mathcal{O}\big(\delta x^2\big)$$

and

$$\bar{\rho}(x_j) = \bar{\rho}_{j+\frac{1}{2}} - \frac{\delta x_{j+\frac{1}{2}}}{2}\,\bar{\rho}'\big(x_{j+\frac{1}{2}}\big) + \mathcal{O}\big(\delta x^2\big).$$

The equalities for $\bar{V}^{\pm}_{j+\frac{1}{2}}$ can be proved by following the same lines. □

With Lemma 2.5 at hand, we can now prove that the approximation of the fluxes can reach second order accuracy in space. Concerning the momentum flux, since the pressure is centered we focus on the convective part $\mathcal{G}^{ML}_{j+\frac{1}{2}}$. We can prove the following result.

Proposition 2.6. *The following equalities hold:*

$$\bar{\mathcal{F}}^{ML}_j = \bar{\rho}(x_j)\bar{V}(x_j) + \mathcal{O}(\delta x^2). \tag{16}$$

$$\bar{\mathcal{G}}^{ML}_{j+\frac{1}{2}} = \bar{\rho}(x_{j+\frac{1}{2}})\bar{V}(x_{j+\frac{1}{2}})^2 + \mathcal{O}(\delta x^2) \tag{17}$$

Proof. By using (5), we start by rewriting the mass flux as follows

$$\bar{\mathcal{F}}^{ML}_j = \frac{\bar{\rho}^+_j + \bar{\rho}^-_j}{2}\bar{V}_j + \frac{\mathcal{F}^{|.|}\left(\bar{\rho}^-_j, \bar{V}_j\right) - \mathcal{F}^{|.|}\left(\bar{\rho}^+_j, \bar{V}_j\right)}{2},$$

where the function $\mathcal{F}^{|.|}$ is defined by $\mathcal{F}^{|.|}(\rho, u) = \mathcal{F}^+(\rho, u) - \mathcal{F}^-(\rho, u) \geqslant 0$. Owing to (13), we readily find that

$$\frac{\bar{\rho}^+_j + \bar{\rho}^-_j}{2}\bar{V}_j = \bar{\rho}(x_j)\bar{V}_j + \mathcal{O}(\delta x^2).$$

Furthermore, since the function $(\rho, V) \mapsto \mathcal{F}^{|.|}(\rho, V)$ is of class $\mathcal{C}^1$ (see [4, Lemma 3.3]), we have

$$\mathcal{F}^{|.|}\left(\bar{\rho}^{\pm}_j, \bar{V}_j\right) = \mathcal{F}^{|.|}\Big(\bar{\rho}(x_j), \bar{V}_j\Big) + \mathcal{O}(\delta x^2).$$

Thus, we find that

$$\frac{\mathcal{F}^{|.|}\left(\bar{\rho}^-_j, \bar{V}_j\right) - \mathcal{F}^{|.|}\left(\bar{\rho}^+_j, \bar{V}_j\right)}{2} = \mathcal{O}(\delta x^2)$$

and (16) is proved.

We turn to momentum flux. By using (14), and bearing in mind definition (9) of $\bar{\mathcal{G}}^{ML}_{j+\frac{1}{2}}$, we first observe that

$$\begin{aligned}\bar{\mathcal{G}}^{ML}_{j+\frac{1}{2}} &= \bar{V}\big(x_{j+\frac{1}{2}}\big)\left(\frac{\bar{\mathcal{F}}^{ML,+}_j + \bar{\mathcal{F}}^{ML,+}_{j+1}}{2} + \frac{\bar{\mathcal{F}}^{ML,-}_j + \bar{\mathcal{F}}^{ML,-}_{j+1}}{2}\right) + \mathcal{O}(\delta x^2),\\ &= \bar{V}\big(x_{j+\frac{1}{2}}\big)\left(\frac{\bar{\mathcal{F}}^{ML}_j + \bar{\mathcal{F}}^{ML}_{j+1}}{2}\right) + \mathcal{O}(\delta x^2).\end{aligned}$$

We then use (16) to find that

$$\bar{\mathcal{G}}^{ML}_{j+\frac{1}{2}} = \bar{V}\big(x_{j+\frac{1}{2}}\big)\left(\frac{\bar{\rho}(x_j)\bar{V}(x_j) + \bar{\rho}(x_{j+1})\bar{V}(x_{j+1})}{2}\right) + \mathcal{O}(\delta x^2).$$

The conclusion (17) is then obtained since we have

$$\frac{\bar{\rho}(x_j)\bar{V}(x_j) + \bar{\rho}(x_{j+1})\bar{V}(x_{j+1})}{2} = \bar{\rho}(x_{j+\frac{1}{2}})\bar{V}(x_{j+\frac{1}{2}}) + \mathcal{O}(\delta x^2).$$

□

The second order accuracy can equally be reached with respect to the time variable, by using the Runge-Kutta discretization (RK2) for approximating the time derivative. Note that this approach may lead to further restriction on the time step in order to preserve the positivity of the density.

3 Higher dimensions: MAC grids

Sec2d

As far as we restrict to Cartesian grids, our approach can be easily extended to higher dimensions, by using the principles of MAC grids. Let us explain how it works in dimension two. The computational domain is the square

$$\Omega = [a_x, b_x] \times [a_y, b_y] \subset \mathbb{R}^2,$$

and we thus aim at writing the scheme for the PDE system

$$\partial_t \begin{pmatrix} \rho \\ \rho u \\ \rho v \end{pmatrix} + \partial_x \begin{pmatrix} \rho u \\ \rho u^2 + p(\rho) \\ \rho uv \end{pmatrix} + \partial_y \begin{pmatrix} \rho v \\ \rho vu \\ \rho v^2 + p(\rho) \end{pmatrix} = 0.$$

We define the meshes as follows

- the primal mesh is defined by the points

$$a_x = x_1 < x_2 < ... < x_{i-1} < x_i < x_{i+1} < ... < x_M < x_{M+1} = b_x,$$

  and

$$a_y = y_1 < y_2 < ... < y_{j-1} < y_j < y_{j+1} < ... < y_N < y_{N+1} = b_y.$$

- then we define the midpoints

$$x_{i+\frac{1}{2}} = \frac{x_i + x_{i+1}}{2},\ \forall i \in [\![1, M]\!], \quad \text{and} \quad y_{j+\frac{1}{2}} = \frac{y_j + y_{j+1}}{2},\ \forall j \in [\![1, N]\!].$$

- We set $\delta x_{i+\frac{1}{2}}$, $\delta y_{j+\frac{1}{2}}$,δx_i et δy_j the length of $[x_i, x_{i+1}]$, $[y_j, y_{j+1}]$, $[x_{i-\frac{1}{2}}, x_{i+\frac{1}{2}}]$ and $[y_{j-\frac{1}{2}}, y_{j+\frac{1}{2}}]$ respectively.

According to the pioneering approach for incompressible flows in [23], we store the discrete densities, the horizontal and the vertical velocities at different locations, see Fig. 3:

HW

Fig:MAC

- the density ρ is evaluated at the centers of the primal cells: we are dealing with the numerical unknowns $\rho_{i+\frac{1}{2},j+\frac{1}{2}}$,
- the horizontal velocity u is evaluated at the centers of the cells $[x_{i-\frac{1}{2}}, x_{i+\frac{1}{2}}] \times [y_j, y_{j+1}]$: the numerical unknowns thus reads $u_{i,j+\frac{1}{2}}$
- the vertical velocity v is evaluated at the centers of the cells $[x_i, x_{i+1}] \times [y_{j-\frac{1}{2}}, y_{j+\frac{1}{2}}]$: the numerical unknowns thus reads $v_{i+\frac{1}{2},j}$.

As in 1D, we need an approximation of ρ at the edges of the primal mesh,

$$\rho_{i,j+\frac{1}{2}} = \frac{\delta x_{i+\frac{1}{2}} \rho_{i+\frac{1}{2},j+\frac{1}{2}} + \delta x_{i-\frac{1}{2}} \rho_{i-\frac{1}{2},j+\frac{1}{2}}}{2\delta x_i}, \text{ and } \rho_{i+\frac{1}{2},j} = \frac{\delta y_{j+\frac{1}{2}} \rho_{i+\frac{1}{2},j+\frac{1}{2}} + \delta y_{j-\frac{1}{2}} \rho_{i+\frac{1}{2},j-\frac{1}{2}}}{2\delta y_j}.$$

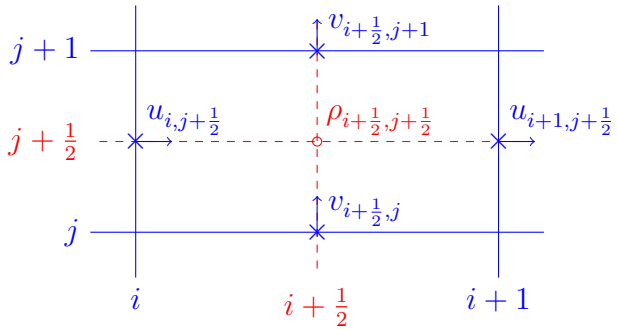

Fig:MAC

Figure 3: Position of the unknowns on a MAC grid.

The first order scheme is a direct extention of the one proposed in BGM2 [5] to the 2D framework. First, the discrete densities $\rho^k_{i+\frac{1}{2},j+\frac{1}{2}}$, $i \in [\![1, M]\!]$, $j \in [\![1, N]\!]$, are updated using the following explicit scheme

$$\frac{\rho^{k+1}_{i+\frac{1}{2},j+\frac{1}{2}} - \rho^k_{i+\frac{1}{2},j+\frac{1}{2}}}{\delta t} + \frac{\mathcal{F}^{\rho,x,k}_{i+1,j+\frac{1}{2}} - \mathcal{F}^{\rho,x,k}_{i,j+\frac{1}{2}}}{\delta x_{i+\frac{1}{2}}} + \frac{\mathcal{F}^{\rho,y,k}_{i+\frac{1}{2},j+1} - \mathcal{F}^{\rho,y,k}_{i+\frac{1}{2},j}}{\delta y_{j+\frac{1}{2}}} = 0.$$

For the sake of simplicity, we skip the superscript k in the sequel. The discrete mass fluxes in the x direction $\mathcal{F}^{\rho,x}_{i,j+\frac{1}{2}}$ are defined, for each value of $j \in [\![1, N]\!]$, as the 1D fluxes, using the values of the horizontal velocity $u_{i,j+\frac{1}{2}}$ to upwind the density in the horizontal direction

$$\mathcal{F}^{\rho,x}_{i,j+\frac{1}{2}} = \mathcal{F}^{\rho,x,+}_{i,j+\frac{1}{2}} + \mathcal{F}^{\rho,x,-}_{i,j+\frac{1}{2}}, \quad \forall (i,j) \in [\![2, M]\!] \times [\![1, N]\!],$$

$$\text{with } \mathcal{F}^{\rho,x,+}_{i,j+\frac{1}{2}} = \mathcal{F}^{+}(\rho_{i-\frac{1}{2},j+\frac{1}{2}}, u_{i,j+\frac{1}{2}}) \quad \text{and} \quad \mathcal{F}^{\rho,x,-}_{i,j+\frac{1}{2}} = \mathcal{F}^{-}(\rho_{i+\frac{1}{2},j+\frac{1}{2}}, u_{i,j+\frac{1}{2}}).$$

Symmetrically, the mass fluxes $\mathcal{F}^{\rho,y}_{i+\frac{1}{2},j}$ in the y direction are defined using the values of the vertical velocity $v_{i+\frac{1}{2},j}$ to upwind the density in the vertical direction

$$\mathcal{F}^{\rho,y}_{i+\frac{1}{2},j} = \mathcal{F}^{\rho,y,+}_{i+\frac{1}{2},j} + \mathcal{F}^{\rho,y,-}_{i+\frac{1}{2},j}, \quad \forall (i,j) \in [\![1,M]\!] \times [\![2,N]\!],$$

$$\text{with } \mathcal{F}^{\rho,y,+}_{i+\frac{1}{2},j} = \mathcal{F}^{+}(\rho_{i+\frac{1}{2},j-\frac{1}{2}}, v_{i+\frac{1}{2},j}) \quad \text{and} \quad \mathcal{F}^{\rho,y,-}_{i+\frac{1}{2},j} = \mathcal{F}^{-}(\rho_{i+\frac{1}{2},j+\frac{1}{2}}, v_{i+\frac{1}{2},j}).$$

For boundary values, we use here zero fluxes: $\mathcal{F}^{\rho,x}_{1,j+\frac{1}{2}} = 0 = \mathcal{F}^{\rho,x}_{M+1,j+\frac{1}{2}}$ and $\mathcal{F}^{\rho,y}_{i+\frac{1}{2},1} = 0 = \mathcal{F}^{\rho,y}_{i+\frac{1}{2},N+1}$.

Next, the horizontal velocities $u^k_{i,j+\frac{1}{2}}$, $i \in [\![2,M]\!]$, $j \in [\![1,N]\!]$ are updated with the following scheme

$$\frac{\rho^{k+1}_{i,j+\frac{1}{2}} u^{k+1}_{i,j+\frac{1}{2}} - \rho^{k}_{i,j+\frac{1}{2}} u^{k}_{i,j+\frac{1}{2}}}{\delta t} + \frac{\mathcal{F}^{u,x,k}_{i+\frac{1}{2},j+\frac{1}{2}} - \mathcal{F}^{u,x,k}_{i-\frac{1}{2},j+\frac{1}{2}}}{\delta x_i} + \frac{\mathcal{F}^{u,y,k}_{i,j+1} - \mathcal{F}^{u,y,k}_{i,j}}{\delta y_{j+\frac{1}{2}}} = 0.$$

We omit, as previously, the superscript k in the definition of the fluxes. We would define the fluxes $\mathcal{F}^{u,x,k}_{i+\frac{1}{2},j+\frac{1}{2}}$, resp. $\mathcal{F}^{u,y,k}_{i,j}$, by upwinding the horizontal momentum $(\rho u)_{i+\frac{1}{2},j+\frac{1}{2}}$, resp. $(\rho u)_{i,j}$, with respect to the value of the horizontal velocity $u_{i+\frac{1}{2},j+\frac{1}{2}}$, resp. the vertical velocity $v_{i,j}$. However, on staggered grids, none of these quantities are obviously defined. As in 1D, we have to bear in mind that, when discretizing the mass conservation equation, we already defined a discrete form of the horizontal, resp. vertical, mass flux based on an upwinding of the density (with respect to the horizontal, resp. vertical, velocity). Thus, the upwinding of horizontal momentum can be next obtained by upwinding the horizontal velocity with respect to the "positive" or "negative" part of the mass fluxes. However, horizontal, resp. vertical, mass fluxes are only defined at points $(x_i, y_{j+\frac{1}{2}})$, resp. $(x_{i+\frac{1}{2}}, y_j)$. The first step is thus to define the "positive" and "negative" parts of the horizontal, resp. vertical, mass flux at points $(x_{i+\frac{1}{2}}, y_{j+\frac{1}{2}})$, resp. (x_i, y_j). This is done by taking the following mean values

$$\mathcal{F}^{\rho,x,\pm}_{i+\frac{1}{2},j+\frac{1}{2}} = \frac{1}{2}\left(\mathcal{F}^{\rho,x,\pm}_{i,j+\frac{1}{2}} + \mathcal{F}^{\rho,x,\pm}_{i+1,j+\frac{1}{2}}\right) \quad \text{and} \quad \mathcal{F}^{\rho,y,\pm}_{i,j} = \frac{\delta x_{i+\frac{1}{2}} \mathcal{F}^{\rho,y,\pm}_{i+\frac{1}{2},j} + \delta x_{i-\frac{1}{2}} \mathcal{F}^{\rho,y,\pm}_{i-\frac{1}{2},j}}{2\delta x_i}.$$

Next, for each $j \in [\![1,N]\!]$, the momentum fluxes $\mathcal{F}^{u,x}_{i+\frac{1}{2},j+\frac{1}{2}}$ are defined, as in 1D, by

$$\mathcal{F}^{u,x}_{i+\frac{1}{2},j+\frac{1}{2}} = u_{i,j+\frac{1}{2}} \mathcal{F}^{\rho,x,+}_{i+\frac{1}{2},j+\frac{1}{2}} + u_{i+1,j+\frac{1}{2}} \mathcal{F}^{\rho,x,-}_{i+\frac{1}{2},j+\frac{1}{2}} + p(\rho_{i+\frac{1}{2},j+\frac{1}{2}}), \quad \forall i \in [\![2,M-1]\!].$$

For boundary fluxes, as in 1D, we use slightly different definitions

$$\mathcal{F}^{u,x}_{\frac{3}{2},j+\frac{1}{2}} = \frac{u_{2,j+\frac{1}{2}}}{2} \mathcal{F}^{\rho,x,-}_{2,j+\frac{1}{2}} + p(\rho_{\frac{3}{2},j+\frac{1}{2}}), \text{ and } \mathcal{F}^{u,x}_{M+\frac{1}{2},j+\frac{1}{2}} = \frac{u_{M,j+\frac{1}{2}}}{2} \mathcal{F}^{\rho,x,+}_{M,j+\frac{1}{2}} + p(\rho_{M+\frac{1}{2},j+\frac{1}{2}}).$$

The fluxes $\mathcal{F}^{u,y}_{i,j}$, for any $(i,j) \in [\![2,M]\!] \times [\![2,N]\!]$ are defined by

$$\mathcal{F}^{u,y}_{i,j} = u_{i,j-\frac{1}{2}} \mathcal{F}^{\rho,y,+}_{i,j} + u_{i,j+\frac{1}{2}} \mathcal{F}^{\rho,y,-}_{i,j}.$$

For the boundary values, we set $\mathcal{F}^{u,y}_{i,1} = 0$ and $\mathcal{F}^{u,y}_{i,N+1} = 0$ for all $j \in [\![2, N]\!]$. Fig. 4 illustrate this construction by putting forward the mass fluxes used in the definition of the momentum flux $\mathcal{F}^{u,x}_{i+\frac{1}{2},j+\frac{1}{2}}$ and $\mathcal{F}^{u,y}_{i,j}$.

Finally, symmetrically, the vertical velocity $v^k_{i+\frac{1}{2},j}$, $i \in [\![1, M]\!]$, $j \in [\![2, N]\!]$ is updated with the following scheme

$$\frac{\rho^{k+1}_{i+\frac{1}{2},j} v^{k+1}_{i+\frac{1}{2},j} - \rho^k_{i+\frac{1}{2},j} v^k_{i+\frac{1}{2},j}}{\delta t} + \frac{\mathcal{F}^{v,x,k}_{i+1,j} - \mathcal{F}^{v,x,k}_{i,j}}{\delta x_{i+\frac{1}{2}}} + \frac{\mathcal{F}^{v,y,k}_{i+\frac{1}{2},j+\frac{1}{2}} - \mathcal{F}^{v,y,k}_{i+\frac{1}{2},j-\frac{1}{2}}}{\delta y_j} = 0.$$

The momentum fluxes $\mathcal{F}^{v,x}$ and $\mathcal{F}^{v,y}$ are defined like $\mathcal{F}^{u,x}$ and $\mathcal{F}^{u,y}$ by inverting the roles played by u and v and by i and j.

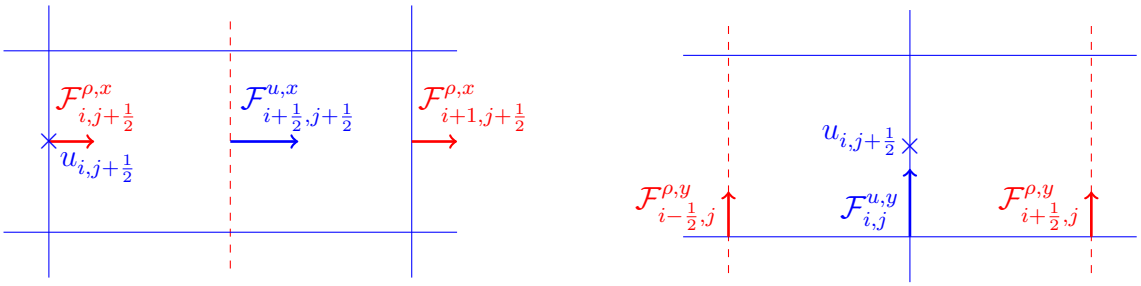

(a) Flux $\mathcal{F}^{u,x}_{i+\frac{1}{2},j+\frac{1}{2}}$ (b) Flux $\mathcal{F}^{u,y}_{i,j}$

Figure 4: Mass flux used in the definition of momentum fluxes.

It can be shown that under a CFL condition — which can be readily deduced from the 1D statement — the positivity of ρ is preserved. Similarly, strengthened assumptions can be identified to guaranty that the decay of the global entropy under suitable stability constraints is still valid on MAC meshes, see [3].

We now turn to explain how to extend the second order scheme to the 2D framework. We apply the 1D MUSCL method to the rows or the columns of the physical variables.

- To define the upgraded mass flux $\mathcal{F}^{\rho,x,ML}$ we use a MUSCL reconstruction only on the columns of the density ρ :

$$\mathcal{F}^{\rho,x,ML}_{i,j+\frac{1}{2}} = \mathcal{F}^+(\rho^-_{i,j+\frac{1}{2}}, u_{i,j+\frac{1}{2}}) + \mathcal{F}^-(\rho^+_{i,j+\frac{1}{2}}, u_{i,j+\frac{1}{2}}).$$

- To define the upgraded mass flux $\mathcal{F}^{\rho,y,ML}$ we use a MUSCL reconstruction only on the rows of the density ρ.

With this new definition of the mass flux $\mathcal{F}^{\rho,x,ML}$ and $\mathcal{F}^{\rho,y,ML}$ we define the new momentum flux $\mathcal{F}^{u,x,ML}$ and $\mathcal{F}^{u,y,ML}$:

- To define the upgraded mass flux $\mathcal{F}^{u,x,ML}$ we use a MUSCL reconstruction only on the columns of the velocity u:

$$\begin{aligned}\mathcal{F}^{u,x,ML}_{i+\frac{1}{2},j+\frac{1}{2}} &= \frac{u^-_{i+\frac{1}{2},j+\frac{1}{2}}}{2}\left(\mathcal{F}^{\rho,x,ML,+}_{i+1,j+\frac{1}{2}}+\mathcal{F}^{\rho,x,ML,+}_{i,j+\frac{1}{2}}\right)\\ &\quad+\frac{u^+_{i+\frac{1}{2},j+\frac{1}{2}}}{2}\left(\mathcal{F}^{\rho,x,ML,-}_{i+1,j+\frac{1}{2}}+\mathcal{F}^{\rho,x,ML,-}_{i,j+\frac{1}{2}}\right)\end{aligned}$$

- To define the upgraded mass flux $\mathcal{F}^{u,y,ML}$ we use a MUSCL reconstruction only on the rows of the velocity u.

The stability and consistency analysis performed in 1D generalize directly to higher dimensions on MAC meshes.

4 Numerical simulations

Simul

4.1 Validation in 1D: manufactured solution

In order to numerically validate the abilities of the MUSCL-like approach, we compute the solutions of the 1D problem

$$\partial_t\begin{pmatrix}\rho\\ \rho u\end{pmatrix}+\partial_x\begin{pmatrix}\rho u\\ \rho u^2+p(\rho)\end{pmatrix}=\begin{pmatrix}0\\ f\end{pmatrix},$$

where the force field $(x,t)\mapsto f(x,t)$ is tailored so that the solution reads

$$\begin{cases}\rho(x,t)=\dfrac{\rho_0(x)e^t}{\left(x+e^t(1-x)\right)^2}\\ u(x,t)=x(1-x).\end{cases}$$

In what follows we simply choose $\rho_0(x)=1$. The solution is smooth and we can expect a full benefit of the MUSCL approach. The computational domain is the slab $[0,1]$ and we perform the simulation for $t\in[0,0.5]$. In the definition of the fluxes, we make use of the SuperBee flux limiter (see example exe 2.1 for the definition).

4.1.1 Uniform mesh and $p(\rho)=\lambda\rho^\gamma$

In Fig. FEx1 5 we plot the L^2-norm of the solution (ρ,u) for several numbers J of grid points and $\delta t=10^{-5}$ (the stability condition is satisfied for all J's of the test). The solution produced by the first order scheme of BGM [4] is referred to by the index SML (in red) and the new scheme is identified with the index ML (in blue). Note that the scheme is order one in time here. We clearly observe the gain of accuracy with the MUSCL scheme: it reaches the second order for both the density (slopes $+$) and the velocity (slopes $\circ$), while the SML scheme approaches the solution at first order only.

It is also worth discussing the interest of replacing the standard Euler scheme by the RK2 method for the time discretization. Hence, for the given mesh size $J=800$,

and using the MUSCL version of the scheme for the space discretization, we make the time step vary $\delta t \in \{1.10^{-4};\ 5.10^{-5};\ 2,5.10^{-5}; 1,25.10^{-5}\}$. Results are displayed in Fig. 6: we observe a slope of order 1 with the Euler scheme (in red), while with RK2 (in blue) we have no slope at all: the error due to the time discretization is hidden by the error in space. Since it does not induce additional computational cost, there is a clear advantage in using the RK2 scheme.

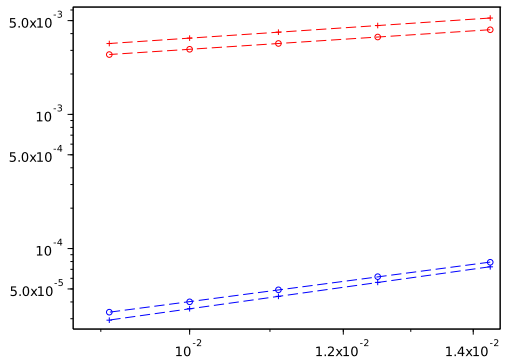

Figure 5: Comparison first order and MUSCL schemes on a smooth solution. Space slopes:
$\rho_{ML} = 2.025$ and $\rho_{SML} = 0.968$,
$u_{ML} = 1.902$ and $u_{SML} = 0.948$.

FEx1

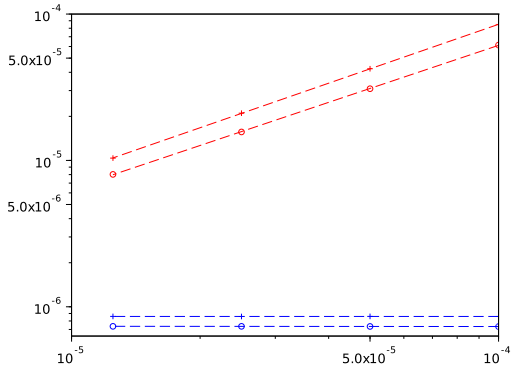

Figure 6: Comparison Euler scheme and RK2 on a smooth solution (MUSCL fluxes). Time slopes:
$\rho_{RK2} = 0$ and $\rho_{EE} = 1.042$,
$u_{RK2} = 0$ and $u_{EE} = 0.924$.

FEx5

4.1.2 Comparison between uniform and non–uniform meshes

We next apply the method on non–uniform meshes for the same tailored solution. To construct non–uniform meshes, we proceed as follows: we randomly pick J points that define a non uniform discretization of the computational domain; then, we split each cell $[x_j, x_{j+1}]$ in its middle $x_{j+\frac{1}{2}}$ to obtain a discretization — still non-uniform — with $2J$ points. Fig. 7 and 8 show the density and velocity error slopes for a time step $\delta t = 10^{-6}$ and four different space–discretizations: $J = 100$, $J = 200$, $J = 400$ and $J = 800$. The symbol + corresponds to the density and $\circ$ to the velocity. Red is still for the MUSCL scheme and blue for the first order method. The convergence rate is the same on uniform and non-uniform meshes, in agreement with Lemma 2.6.

FEx1-reg FEx1-irreg

lem:snd_order

4.1.3 Uniform mesh and $p(\rho) = \frac{(\gamma-1)^2}{4\gamma}\left(\frac{\rho}{\rho^*-\rho}\right)^\gamma$

We finally check the ability of the scheme in dealing with a more complex pressure law. The tailored solution is still the same, but now we set $p(\rho) = k\left(\frac{\rho}{\rho^*-\rho}\right)^\gamma$ where $k = \frac{(\gamma-1)^2}{4\gamma}$. This is a particular case of the Van der Waals state law, it arises in the modeling of dusty gases for instance. We point out that this pressure law does not lead

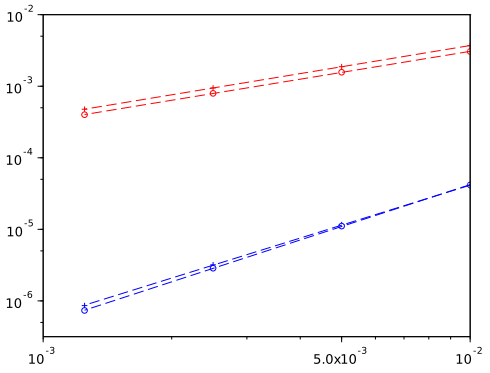

Figure 7: Slopes on uniform meshes for a smooth solution:
$\rho_{ML} = 1.86$ and $\rho_{SML} = 0.99$,
$u_{ML} = 1.94$ and $u_{SML} = 0.98$.

FEx1-reg

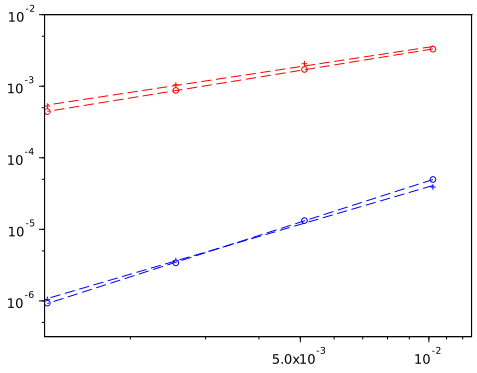

Figure 8: Slopes on non–uniform meshes for a smooth solution:
$\rho_{ML} = 1.75$ and $\rho_{SML} = 0.9$,
$u_{ML} = 1.92$ and $u_{SML} = 0.97$.

FEx1-irreg

to any difficulty in the design of the scheme and its consistency properties apply equally well to this case. Tests are performed with $\gamma = 0.6$ and $\rho^* = 3$. Note that admissible densities should remain in the domain $0 \leq \rho < \rho^*$; this issue is further discussed in Section 4.2.2 below. Fig. 9 shows the slope of the error (the legend is still the same): for the smooth solution considered here, the convergence rate is still second–order.

subVdW

FEx1-waals

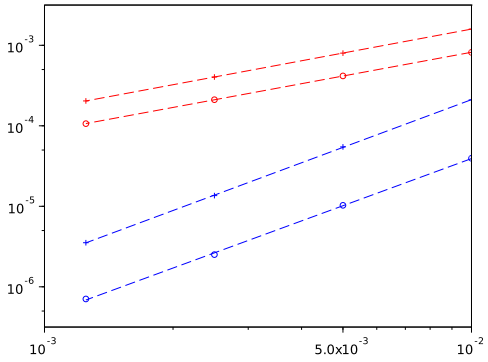

Figure 9: Convergence for a smooth solution, Van der Waals law. Space slopes: $\rho_{ML} = 1.97$ and $\rho_{SML} = 0.99$, $u_{ML} = 1.95$ and $u_{SML} = 0.98$.

FEx1-waals

4.2 Validation in 1D: Riemann problems

4.2.1 Pressure law $p(\rho) = a\rho^\gamma$

Now that we have validated the second order accuracy of the method on a smooth enough solution, we study the behavior of the scheme with discontinuous solutions. We consider Riemann problems on a computational domain $[a, b]$: the initial data has a jump located at $a < x = 0 < b$; we denote by (ρ_l, u_l) and (ρ_r, u_r) the left and right states for the density/velocity pair, respectively. The pressure law is defined by $\gamma = 1.6$ and $a = \frac{(\gamma-1)^2}{4\gamma}$. The flux limiter that we use is the SuperBee one and the others data are given in the following table.

Figure	Problem	a	b	ρ_l	ρ_r	u_l	u_r
Fig. 10	Rarefaction-Rarefaction	-0.7	0.3	0.5	1	-0.5	-0.2
Fig. 11	Shock-Schock	-0.2	0.8	1	2	1	0.25
Fig. 12	Rarefaction-Shock	-0.7	0.3	1	0.5	-0.5	-0.5
Fig. 13	Vacuum	-0.5	0.5	1	01	-5	5

In Fig 10 to 13, the MUSCL–like method (ML) is represented with a continuous line and the method without MUSCL (SML) is plotted with a dashed line. The colors refer to discretization: blue for $J = 800$, red for $J = 1600$ and green for $J = 3200$. As previously, red slopes are for the quantities SML and blue for the quantities ML, $+$ is for the density and $\circ$ for the velocity. Of course the solutions of Riemann problems are not smooth and the consistency analysis does not apply. Nevertheless, we clearly see that using the MUSCL–like method provides better results than the first order method as the error is smaller with the MUSCL fluxes.

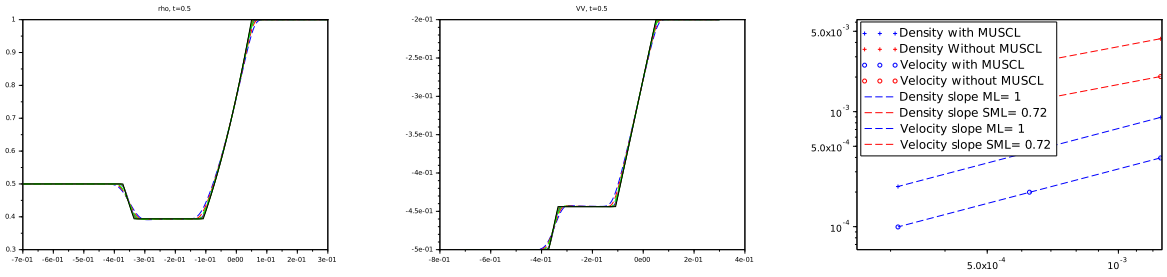

Figure 10: Riemann problems. Slopes: $\rho_{ML} = 1$ and $\rho_{SML} = 0.72$, $u_{ML} = 1$ and $u_{SML} = 0.72$.

FEx6

4.2.2 Riemann problems for a Van der Waals pressure law

subVdW

As already said above, our method does not rely on the resolution of Riemann problems, and the numerical fluxes have a simple expression for very general pressure laws, while the scheme is entropy–decaying. For instance the scheme is still efficient for Van der

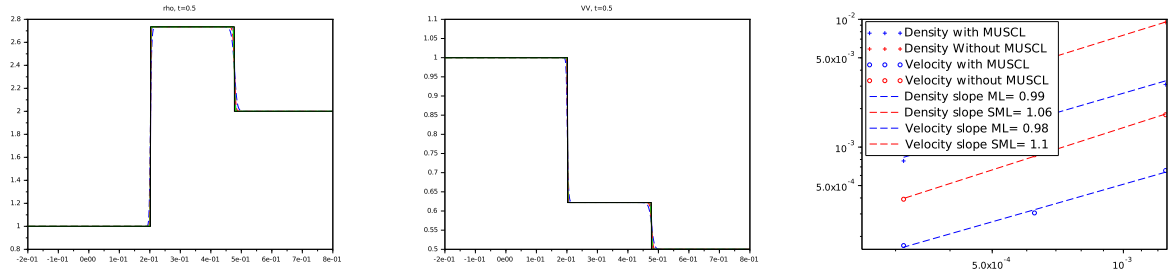

Figure 11: Riemann problems. Slopes: $\rho_{ML} = 0.99$ and $\rho_{SML} = 1.06$, $u_{ML} = 0.98$ and $u_{SML} = 1.1$.

FEx7

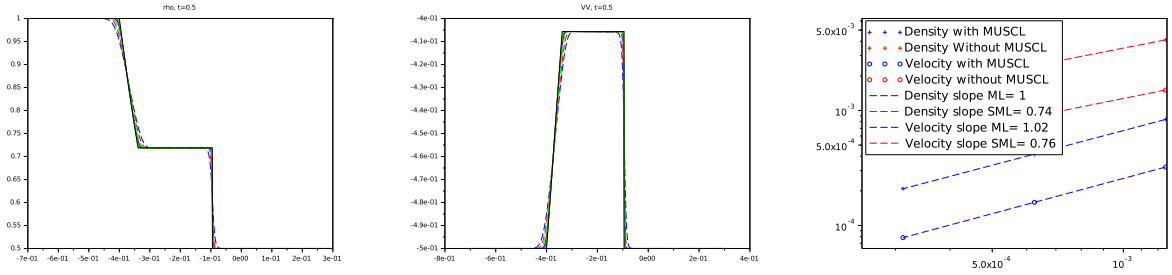

Figure 12: Riemann problems. Slopes: $\rho_{ML} = 1$ and $\rho_{SML} = 0.74$, $u_{ML} = 1.02$ and $u_{SML} = 0.76$

FEx8

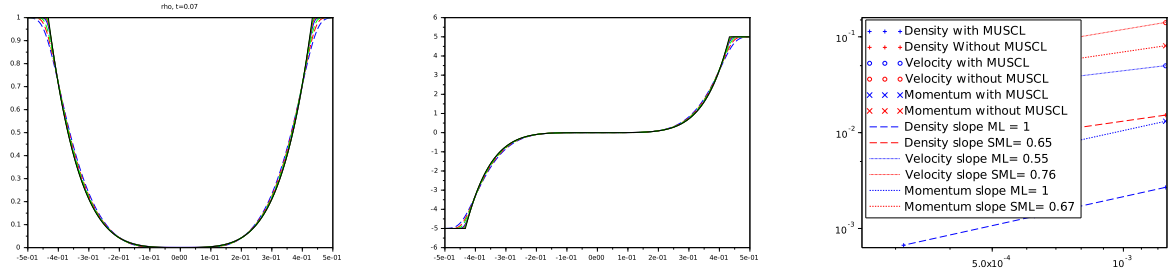

Figure 13: Riemann problems. Slopes: $\rho_{ML} = 1$ and $\rho_{SML} = 0.65$, $u_{ML} = 0.55$ and $u_{SML} = 0.76$,
$\rho u_{ML} = 1$ and $\rho u_{SML} = 0.67$.

FEx9

Waals–like laws $p(\rho) = \frac{(\gamma-1)^2}{4\gamma}\frac{\rho^\gamma}{\rho^*-\rho}$. Such a relation is intended to retain some packing effects that prevent the density to exceed the threshold $\rho^\star$. However the preservation of this constraint by the numerical unknown leads to a strengthened stability condition, see [BGM2, 5, Prop. 5]. For the MUSCL version of the scheme the stability condition takes the following form.

Rho-*

Proposition 4.1 (Close-packing threshold)**.** *Suppose that the initial data satisfies* $\rho^0_{j+\frac{1}{2}} \leq$

$\rho^\star$ *for all* $j \in [\![1, J]\!]$. *We assume the CFL-like condition*

$$\frac{\delta t}{\delta x_{j+\frac12}} \left(\left[\lambda_+(\rho_j^{k,-}, V_j^k) \right]^+ + \left[\lambda_-(\rho_{j+1}^{k,+}, V_{j+1}^k) \right]^- \right) \leqslant \frac12 \left(1 - \frac{\rho^k_{j+\frac12}}{\rho^\star} \right), \quad \forall j \in [\![1, J]\!],$$

at every time step. Then $\rho^{k+1}_{j+\frac12} \leq \rho^\star$ *for all* $j \in [\![1, J]\!]$ *and* $k \in \mathbb{N}$.

Proof. We have

$$\begin{aligned}
\rho^{k+1}_{j+\frac12} &= \rho^k_{j+\frac12} + \frac{\delta t}{\delta x_{j+\frac12}} \left(\mathcal{F}^-(\rho_j^{k,+}, V_j^k) - \mathcal{F}^+(\rho_{j+1}^{k,-}, V_{j+1}^k) \right) \\
&\qquad + \frac{\delta t}{\delta x_{j+\frac12}} \left(\mathcal{F}^+(\rho_j^{k,-}, V_j^k) - \mathcal{F}^-(\rho_{j+1}^{k,+}, V_{j+1}^k) \right) \\
&\leq \rho^k_{j+\frac12} + \frac{\delta t}{\delta x_{j+\frac12}} \left(\mathcal{F}^+(\rho_j^{k,-}, V_j^k) - \mathcal{F}^-(\rho_{j+1}^{k,+}, V_{j+1}^k) \right) \\
&\leq \rho^k_{j+\frac12} + \frac{\delta t}{\delta x_{j+\frac12}} \left(\rho_j^{k,-} \left[\lambda_+(\rho_j^{k,-}, V_j^k) \right]^+ + \rho_{j+1}^{k,+} \left[\lambda_-(\rho_{j+1}^{k,+}, V_{j+1}^k) \right]^- \right).
\end{aligned}$$

Let us assume $\rho^k_{j+\frac12} \leq \rho^\star$ for any j; then $\rho_j^{k,\pm} \leq 2\rho^\star$ (see the proof of Proposition 2.3). Let us introduce

$$\epsilon^k_{j+\frac12} = 1 - \frac{\rho^k_{j+\frac12}}{\rho^\star}.$$

We get

$$\rho^{k+1}_{j+\frac12} \leq \rho^\star - \rho^\star \left(\epsilon^k_{j+\frac12} - \frac{2\delta t}{\delta x_{j+\frac12}} \left(\left[\lambda_+(\rho_j^{k,-}, V_j^k) \right]^+ + \left[\lambda_-(\rho_{j+1}^{k,+}, V_{j+1}^k) \right]^- \right) \right).$$

Finally, assuming

$$\epsilon^k_{j+\frac12} \geq \frac{2\delta t}{\delta x_{j+\frac12}} \left(\left[\lambda_+(\rho_j^{k,-}, V_j^k) \right]^+ + \left[\lambda_-(\rho_{j+1}^{k,+}, V_{j+1}^k) \right]^- \right)$$

we obtain $\rho^{k+1}_{j+\frac12} \leq \rho^\star$ for any j. □

As observed for the maximum principle, the CFL-like condition for the MUSCL scheme is twice more constrained than with the first order scheme. This is still due to the bound from below $\rho_j^+ \leq 2\rho_{j+\frac12}$ and $\rho_{j+1}^- \leq 2\rho_{j+\frac12}$.

This condition is much more demanding than the standard CFL condition, which is enough to preserve the bounds on the density when using a more standard scheme, say for instance based on the the Lax–Friedrichs flux. (Note that the analysis uses crucially the convexity of the invariant domain of the PDE, see [8, Section 2.2.1 & Prop. 2.11], and it does not apply when the invariant regions are non–convex, see e.g. [11].) However, the scheme based on the kinetic fluxes is far less diffusive than Lax–Friedrichs' method, so that it finally competes in terms of numerical effort for a given numerical accuracy.

To illustrate the difficulty, we go back to the numerical tests proposed in [BGM2, Section 4.1]:

- $\rho_l = \rho_r = \frac{1}{3}$ and $\rho^\star = 1$
- $u_l = V_{abs}$ and $u_r = -V_{abs}$
- $\gamma = 2$
- $[a, b] = [-0.5; 0.5]$ and $J = 200$
- $T = 0.1$.
- Φ =MinMod

The following table shows that for a given time step, the accuracy is far better with our scheme (even in its first order version) than with Lax-Friedrichs. Solutions are displayed in Fig. 14 and Fig. 15: for the same numerical conditions δt and δx, the Lax–Friedrichs scheme produces much more numerical diffusion and the solution is poorly captured.

V_{abs}	δt	$\lvert\rho_{ML} - \rho_{ex}\rvert$	$\lvert\rho_{SML} - \rho_{ex}\rvert$	$\lvert\rho_{LF} - \rho_{ex}\rvert$
0.5	$2,45.10^{-3}$	$2,67.10^{-3}$	$3,03.10^{-3}$	$0,63$
1	$6,6.10^{-4}$	$2,99.10^{-3}$	$3,53.10^{-3}$	$0,98$
1.5	$2,1.10^{-4}$	$3,50.10^{-3}$	$3,94.10^{-3}$	$1,46$
2	$8,1.10^{-4}$	$3,36.10^{-3}$	$3,73.10^{-3}$	$2,12$

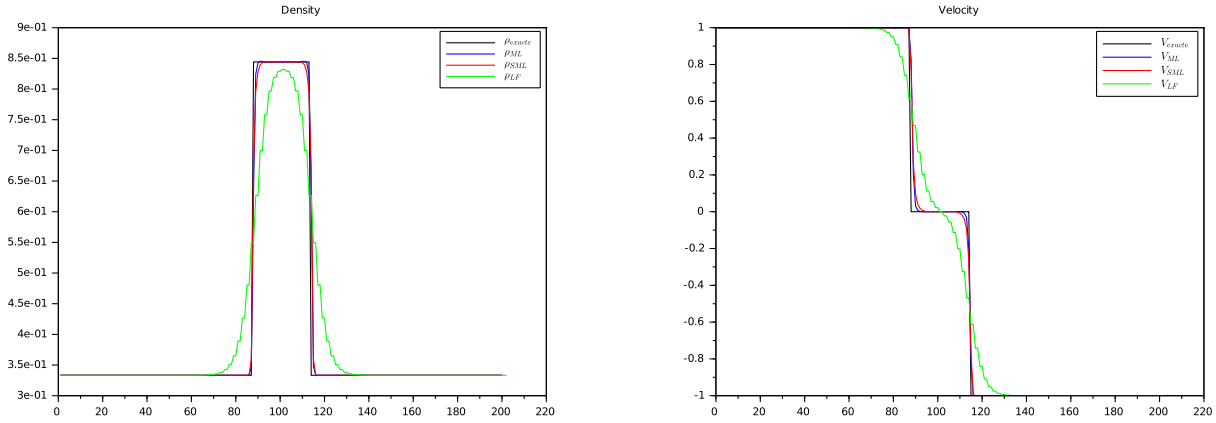

Figure 14: Barotropic gas with Van der Waals law: comparison of the kinetic scheme (1st and 2nd order) with the Lax–Freidrichs scheme. Density and Velocity solutions for $V_{abs} = 1$.

We end this section by illustrating the result of Proposition 4.1: we perform simulations for different values of $V_{abs} \in \{0.5, 0.75, 1, 1.25, 1.5, 1.75, 2, 2.25, 2.5\}$ and different values of the time step δt. For each values of V_{abs}, we select the largest value of δt which yields an "admissible" result (in the sense that it remains oscillation–free at $T = 0.1$). In Fig. 16, we plot this selected δt: in a logarithm scale, we obtain a straight line with a slope close to 2, which is consistent with Proposition 4.1 since when ρ becomes close to $\rho^\star$, the characteristic speeds behave like $\left(1 - \frac{\rho_m}{\rho^\star}\right)^{-1}$.

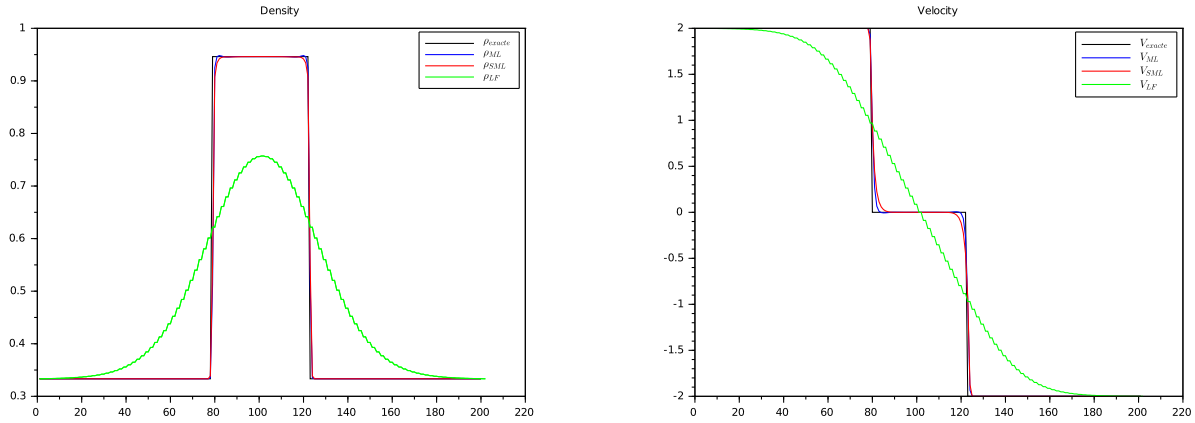

Figure 15: Barotropic gas with Van der Waals law: comparison of the kinetic scheme (1st and 2nd order) with the Lax–Freidrichs scheme. Density and Velocity solutions for $V_{abs} = 2$.

Rho_VV_2

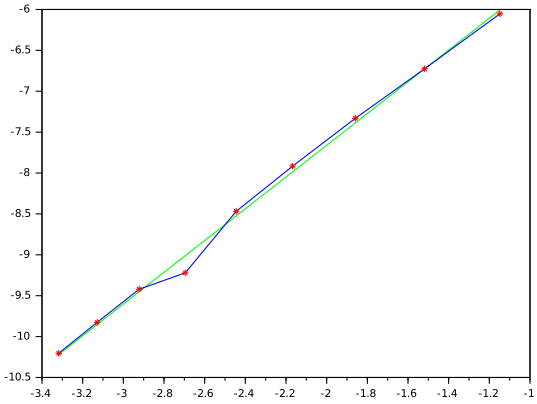

Figure 16: Maximal admissible time step δt as a function of $1 - \frac{\rho_M}{\rho^\star}$ in blue; the green line has a slope 1.94.

MaxAccept

4.3 Numerical simulations in 2D

4.3.1 Falling water columns

We turn to 2D simulation, with a test–case inspired from [1]. We simulate three columns of water falling into a rectangular basin at an initial time (meaning that after the fall at time $t_0 = 0$, there is no source term): the computational domain is the two–dimensional square $[-1, 1] \times [-1, 1]$ and we are using the dimensionless Shallow Water system which amounts to set $p(\rho) = \rho^2$. The PDE system is endowed with reflection boundary

Agu

conditions and the following initial data

$$\begin{cases} \rho(0,x,y) = 3 + \mathbb{1}_{(x-0.5)^2+(y-0.5)^2<(0.15)^2} + \mathbb{1}_{(x+0.5)^2+(y+0.5)^2<(0.15)^2} + 2 \times \mathbb{1}_{x^2+y^2<(0.2)^2}, \\ u(0,x,y) = 0, \\ v(0,x,y) = 0. \end{cases}$$

The simulation in [Agu] is reproduced in Fig. 17: it is based on the second order Nessayhu–Tadmor scheme [NT], coupled to a specific reconstruction procedure which is intended to reduce the numerical diffusion and to capture shocks with an enhanced accuracy. The MUSCL scheme competes with such an approach, as it appears in Fig. 18 on the right (simulations have been performed with the MinMod limiter). Fig. 18 shows the advantages in using the MUSCL method compared to the first order scheme, which, for the same numerical parameters, loses the complex structures of the flow.

In these simulations, the time step is determined by using the relation

$$CFL = 2\frac{\delta t}{\delta x}\lambda_{max}$$

where λ_{max} is the maximum of the waves speed.

Il me semble qu il manque une info ici...: que vaut CFL

As already observed in [Agu], the simulation is quite sensitive to the time step: some oscillations might appear when δt is not small enough.

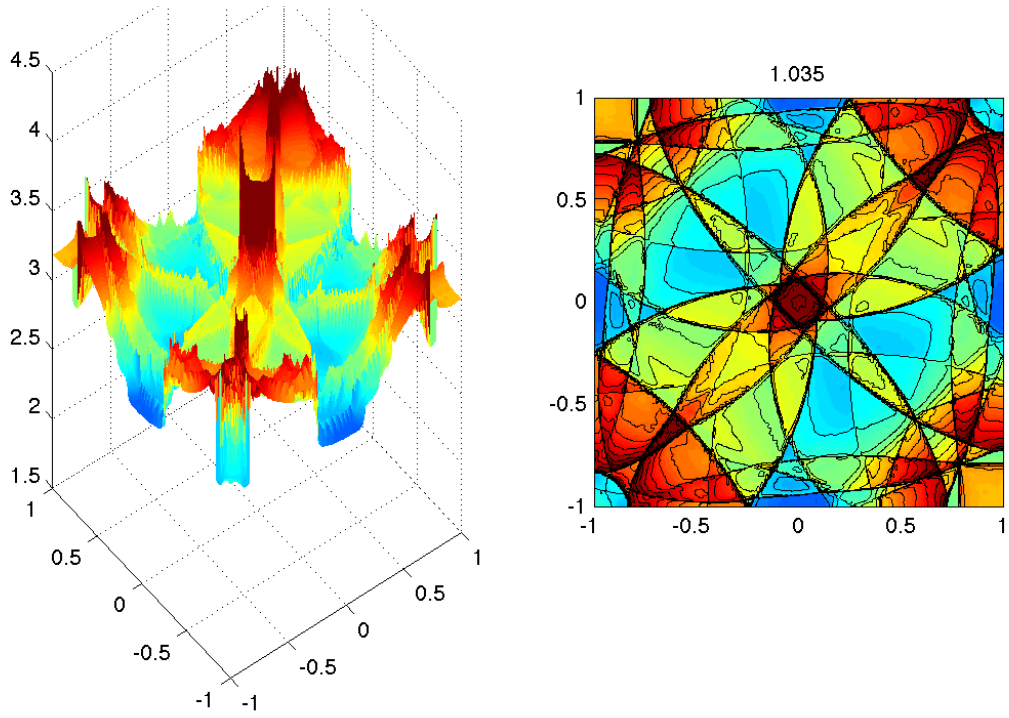

Figure 17: Simulation of the Shallow Water system, by courtesy of N. Aguillon [Agu].

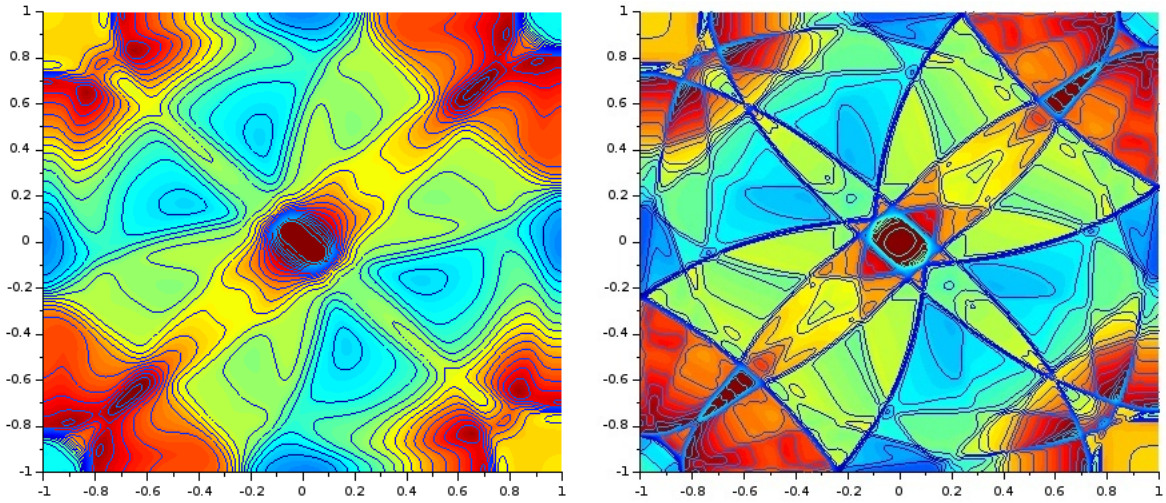

Figure 18: Simulation of the Shallow Water system for $\delta t = 10^{-4}$: Results with the first order scheme (left) and with the MUSCL scheme (right)

S:ours

4.3.2 Forward facing step.

This test case is the wind tunnel with a step, introduced in [CW 15]. The computational domain Ω is the L-shaped domain

$$\Omega = \Omega_0 \setminus \Omega_{step}, \quad \Omega_0 = [0,3] \times [0,1], \quad \Omega_{step} = [0.6,3] \times [0,0.2].$$

The equation of state of the fluid is $p(\rho) = \rho$ and the initial data are given by $\rho = 1$ and $u = (3,0)$. On the top and bottom walls, we use reflection boundary conditions. The flow enters through the left boundary and is free at the outflow (right) section. The rectangle Ω_0 is discretized with a 600×200 Cartesian grid. We take the step into account by removing the mesh points at the right bottom part of the domain, corresponding to the step Ω_{step}. For the simulation reproduced in Fig. [S:step 19] the time steps are respectively

$$\delta t_{SML} = \frac{0.5 \times 0.25}{200} \text{ and } \delta t_{ML} = \frac{\delta t_{SML}}{8}.$$

The results are in agreement with the literature.citer qq un ici We observe that the structures are sharper with the MUSCL scheme.

Acknowledgements

We warmly thank N. Aguillon for invaluable hints about the test cases in her PhD thesis.

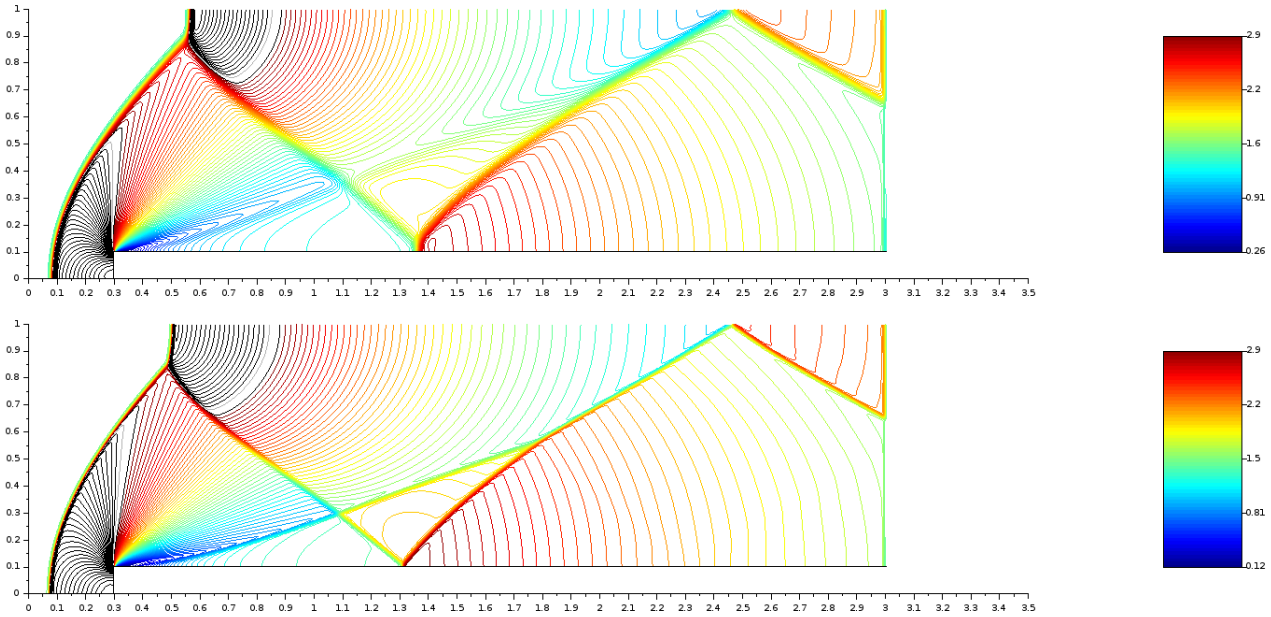

Figure 19: Simulation of the wind tunnel with a step test case: Results with the first order scheme (up) and with the MUSCL scheme (down)

S:step

References

Agu [1] N. Aguillon. *Problèmes d'interfaces et couplages singuliers dans les systèmes hyperboliques : analyse et analyse numérique*. PhD thesis, Univ. Paris Sud, 2014.

BAM [2] M. Berger, M.-J. Aftosmis, and S.-M. Murman. Analysis of slope limiters on irregular grids. *Aerospace Sciences Meeting, Reno, NV, USA*, 43rd AIAA, 2005.

BGM3 [3] F. Berthelin, T. Goudon, and S. Minjeaud. Consistency analysis of a 1D finite volume scheme for barotropic Euler models. In *Finite Volumes for Complex Applications VII; Methods, Theoretical Aspects, and Elliptic, Parabolic and Hyperbolic Problems, Berlin*, volume 77 and 78 of *Springer Proceedings in Mathematics & Statistics*, pages 97–106. Springer, 2014.

BGM [4] F. Berthelin, T. Goudon, and S. Minjeaud. Kinetic schemes on staggered grids for barotropic Euler models: entropy-stability analysis. *Math. Comput.*, 84:2221–2262, 2015.

BGM2 [5] F. Berthelin, T. Goudon, and S. Minjeaud. Multifluid flows: a kinetic approach. *J. Sci. Comput.*, 66(2):792–824, 2016.

BCD2 [6] C. Berthon, Y. Coudière, and V. Desveaux. Development of DDFV methods for the Euler equations. In *Finite Volumes for Complex Applications VI; Methods, Theoretical Aspects, and Elliptic, Parabolic and Hyperbolic Problems, Prague*, volume 4 of *Springer Proceedings in Mathematics & Statistics*, pages 117–124. Springer, 2011.

BCD [7] C. Berthon, Y. Coudière, and V. Desveaux. Second-order MUSCL schemes based on dual mesh gradient reconstruction (DMGR). *ESAIM Math. Model. Numer. Anal.*, 48(2):583–602, 2014.

Bouc [8] F. Bouchut. *Nonlinear stability of finite volume methods for hyperbolic conservation laws and well-balanced schemes for sources*. Frontiers in Math. Birkhauser, 2004.

CCCG [9] C. Calgaro, E. Chane-Kane, E. Creusé, and T. Goudon. L^∞-stability of vertex-based MUSCL finite volume schemes on unstructured grids: simulation of incompressible flows with high density ratios. *J. Comput. Phys.*, 229(17):6027–6046, 2010.

penel [10] C. Calgaro, E. Creusé, T. Goudon, and Y. Penel. Positivity-preserving schemes for Euler equations: sharp and practical CFL conditions. *J. Comput. Phys.*, 234:417–438, 2013.

ChG [11] C. Chalons and P. Goatin. Transport-equilibrium schemes for computing contact discontinuities in traffic flow modeling. *Commun. Math. Sci.*, 5(3):533–551, 2007.

CC [12] S. Clain and V. Clauzon. L^∞ stability of the MUSCL methods. *Numerische Mathematik*, 116:31–64, 2010.

CDNR [13] F. Clarelli, C. Di Russo, N. Natalini, and M. Ribot. Mathematical models for biofilms on the surface of monuments. In *Applied and Industrial Mathematics in Italy III, 9th Conference SIMAI*, volume 82 of *Advances in Mathematics for Applied Sciences*. World Scientific, 2009.

CDNR2 [14] F. Clarelli, C. Di Russo, N. Natalini, and M. Ribot. A fluid dynamics model of the growth of phototrophic biofilms. *J. Math. Biology*, 66(7):1387–408, 2013.

CW [15] P. Colella and P. Woodward. The numerical simulation of two-dimensional fluid flow with strong shocks. *J. Comput. Phys.*, 54:115–173, 1984.

CoPe [16] F. Coron and B. Perthame. Numerical passage from kinetic to fluid equations. *SIAM J. Numer. Anal.*, 28:26–42, 1991.

Daf [17] C. Dafermos. *Hyperbolic conserrvation laws in continuum physics*, volume 325 of *Grundlehren der mathematischen Wissenschaften*. Springer, 2010. Thrid ed.

Desh [18] S. M. Deshpande. Kinetic theory based new upwind methods for inviscid compressible flows. In *AIAA 24th Aerospace Science Meeting, Jan 6-9, 1986, Nevada, USA*, 1986. AIAA paper 86-0275.

Desh2 [19] S. M. Deshpande. On the Maxwellian distribution, symmetric form and entropy conservation for the Euler equations. Technical report, NASA Langley Research Centre, Hampton, VA, 1986. NASA TP2613.

GHK [20] L. Gastaldo, R. Herbin, W. Kheriji, C. Lapuerta, and J.-C. Latché. Staggered discretizations, pressure correction schemes and all speed barotropic flows. In *Finite Volumes for Complex Applications VI, Problems and Perspectives, Prague, Czech Republic*, volume 4, pages 839–855, 2011.

GodR [21] E. Godlewski and P.-A. Raviart. *Numerical approximation of hyperbolic systems of conservation laws*, volume 118 of *Applied Mathematical Sciences*. Springer, New-York, 1996.

JL2 [22] T. Goudon, S. Minjeaud, and J. Llobell. A numerical scheme for the euler equations on staggered grids. Work in preparation.

HW [23] F. H. Harlow and J. E. Welch. Numerical calculation of time-dependent viscous incompressible flow of fluid with free surface. *Phys. Fluids*, 8(12):2182–2189, 1965.

HKL [24] R. Herbin, W. Kheriji, and J.-C. Latché. Staggered schemes for all speed flows. *ESAIM:Proc*, 35:122–150, 2012. Actes du Congrès National de Mathématiques Appliquées et Industrielles.

HLN [25] R. Herbin, J.-C. Latché, and T. T. Nguyen. Explicit staggered schemes for the compressible Euler equations. In *Applied mathematics in Savoie—AMIS 2012: Multiphase flow in industrial and environmental engineering*, volume 40 of *ESAIM Proc.*, pages 83–102. EDP Sci., Les Ulis, 2013.

HLN2 [26] R. Herbin, J.-C. Latché, and T. T. Nguyen. Explicit staggered schemes for the compressible Euler equations. *ESAIM:Proc.*, 40:83–102, 2013.

Kan [27] S. Kaniel and J. Falcovitz. Approximation of the hydrodynamic equations by a transport process. In R. Rautman, editor, *Proceedings of IUTAM Symposium on Approximation Methods for Navier-Stokes Problems*, volume 771 of *Lecture Notes in Math.* Springer-Verlag, 1980.

Leveq [28] R. J. LeVeque. *Finite volume methods for hyperbolic problems.* Cambridge Texts in Applied Mathematics. Cambridge University Press, Cambridge, 2002.

AUSM2 [29] M.-S. Liou. A sequel to AUSM: AUSM+. *J. Comput. Phys.*, 129:364–382, 1996.

AUSM [30] M.-S. Liou and C. J. Steffen Jr. A new flux splitting scheme. *J. Comput. Phys.*, 107:23–39, 1993.

NT [31] H. Nessyahu and E. Tadmor. Non-oscillatory central differencing for hyperbolic conservation laws. *J. Comput. Phys.*, 87(2):408–463, 1990.

PerBS [32] B. Perthame. Second order Boltzmann schemes for compressible Euler equations in one and two space dimension. *SIAM J. Numer. Anal.*, 29(1):1–19, 1992.

Polizzi [33] B. Polizzi. *Modeling and numerical simulations for fluid mechanics systems with constraints; application to biology and road traffic.* PhD thesis, Univ. Côte d'Azur, 2016.

Pullin [34] D. I. Pullin. Direct simulation methods for compressible gas flow. *J. Comput. Phys.*, 34:231–244, 1980.

Swe [35] P. Sweby. High resolution schemes using flux limiters for hyperbolic conservation laws. *SIAM J. Numer. Anal.*, 21(5):995–1011, 1984.

tor-09-rie [36] E. F. Toro. *Riemann solvers and numerical methods for fluid dynamics. A practical introduction.* Springer-Verlag, 2009. 3rd edition.

Wes3 [37] D. R. van der Heul, C. Vuik, and P. Wesseling. A conservative pressure-correction method for flow at all speeds. *Comput. & Fluids*, 32(8):1113–1132, 2003.

BVL [38] B. van Leer. Towards the ultimate conservative difference scheme. V. A second-order sequel to Godunov's method [J. Comput. Phys. **32** (1979), no. 1, 101–136]. *J. Comput. Phys.*, 135(2):227–248, 1997. With an introduction by Ch. Hirsch, Commemoration of the 30th anniversary {of J. Comput. Phys.}.

Hof [39] B. van't Hof and A. E. P. Veldman. Mass, momentum and energy conserving (MaMEC) discretizations on general grids for the compressible Euler and shallow water equations. *J. Comput. Phys.*, 231(14):4723–4744, 2012.

Wes1 [40] I. Wenneker, A. Segal, and P. Wesseling. A Mach-uniform unstructured staggered grid method. *Internat. J. Numer. Methods Fluids*, 40(9):1209–1235, 2002.

Wes2 [41] I. Wenneker, A. Segal, and P. Wesseling. Conservation properties of a new unstructured staggered scheme. *Comput. & Fluids*, 32(1):139–147, 2003.

Zaz [42] C. Zaza. *Contribution à la résolution numérique d'écoulements à tout nombre de Mach et au couplage fluide-poreux en vue de la simulation d'écoulements diphasiques homogénéisés dans les composants nucléaires.* PhD thesis, Univ. Aix–Marseille, 2015.